# Study of polarization properties of light emitted from *a*-plane InGaN/GaN quantum well-based light emitting diodes

Hung-Hsun Huang and Yuh-Renn Wu[a)]
*Graduate Institute of Photonics and Optoelectronics and Department of Electrical Engineering, National Taiwan University, Taipei 10617, Taiwan*

(Received 18 May 2009; accepted 17 June 2009; published online 23 July 2009)

This paper discusses the optical characteristics of a nonpolar *a*-plane InGaN/GaN quantum well with different indium compositions, quantum well widths, and injection carrier densities. The self-consistent Poisson and $6\times6$ $k\cdot p$ Schrödinger solver has been applied to study the band structures in nonpolar *a*-plane InGaN-based quantum well light emitting diodes (LEDs). We find that the larger indium composition and smaller well width make the energy separation of $|Y\rangle$-like state to $|Z\rangle$-like state larger, and as a result enhance the polarization ratio of light. However, the polarization ratio decreases as the carrier injection increases, which might be a drawback for high power applications. We have studied the optimization condition for designing the *a*-plane InGaN quantum well LED for applications, such as liquid crystal display backlight modules and lasers, which would be useful information for device designs. © *2009 American Institute of Physics*. [DOI: 10.1063/1.3176964]

## I. INTRODUCTION

In recent years, III-nitride-based optoelectronic devices, i.e., InGaN/GaN light emitting diodes (LEDs) have been widely used in several areas such as solid state lighting and liquid crystal display (LCD) backlight module. However, there is a strong build-in electric field caused by the spontaneous and piezoelectric polarization charge at the interface of InGaN and GaN, which leads to the quantum-confine Stark effect (QCSE) in the *c*-plane InGaN quantum well. Therefore, there is an obviously spatial separation between electron and hole wave functions due to the huge band bending in the conventional *c*-plane InGaN quantum well, which is a bottleneck of *c*-plane InGaN-based LEDs. In order to eliminate the internal field in quantum well, one of the solutions is growing the InGaN quantum well along the $(11\bar{2}0)$ direction (*a*-plane) or along $(1\bar{1}00)$ direction (*m*-plane),[1] where the polarization charge is not formed at the interface. The advantages of using nonpolar LEDs are not only avoiding the QCSE but also making a polarized light source, which is important in applications needing a polarized light source, such as LCD backlight module.[2] Therefore, we can avoid using polarizers, enhance the power efficiency, and reduce the cost by using nonpolar quantum well LED as a polarization light source.

There have been some works for studying of nonpolar InGaN/GaN quantum well LEDs in theoretical[3–8] and in experimental.[9–19] They observed an in-plane anisotropy polarization feature by photoluminescence and electroluminescence measurements, which are not observed in *c*-plane quantum well. The theoretical studies have also shown the anisotropy strain effect in nonpolar quantum well, which leads to the modification of valence band structure.[20] This modification will directly affect the polarization properties of the emitted light.[3,21]

As we know, the quantum well width has a strong relation to the quantum confinement effect. There is a stronger quantum confinement in a narrower quantum well width. Due to the absence of QCSE in the nonpolar InGaN quantum well, it is possible to make a wider quantum well to increase the amount of carriers injected into the quantum well. However, wider quantum well might reduce the energy separation of each subband[22] so that the polarization ratio might decrease. Also, the compressive strain induced by the lattice mismatch is determined by the quantity of indium alloy, and as the result the LEDs with different emission wavelengths may have different polarization performances. The injected carrier density also plays an important role in determining the light emission property. Usually, with higher carrier injection density, more subbands are filled, and it reduces the polarization ratio as well. Therefore, the polarization ratio also has a strong relation with carrier injection density in the quantum well.[17]

In this work, we applied a self-consistent Poisson and $6\times6$ $k\cdot p$ Schrödinger method[23,24] to solve the band structure, energy subband levels, and wave functions. The strain deformation effect is also considered here. We varied different quantum well widths and indium compositions to design our *a*-plane InGaN quantum well, and studied the polarization light emission properties under different carrier injection conditions.

## II. FORMALISM

To understand the light emission polarization properties of the *a*-plane quantum well system, we need to address the issue of the valence band states mixing. We applied $6\times6$ $k\cdot p$ method[25] for calculating the valence band and effective

[a)]Electronic mail: yrwu@cc.ee.ntu.edu.tw.

 

mass approximation method for calculating the conduction band. The $6\times6$ Hamiltonian of $k\cdot p$ model for $(11\bar{2}0)$ direction can be expressed as

$$H^v = \begin{pmatrix} F & 0 & -H^* & 0 & K^* & 0 \\ 0 & G & \Delta & -H^* & 0 & K^* \\ -H & \Delta & \lambda & 0 & I^* & 0 \\ 0 & -H & 0 & \lambda & \Delta & I^* \\ K & 0 & I & \Delta & G & 0 \\ 0 & K & 0 & I & 0 & F \end{pmatrix}, \tag{1}$$

where

$$F = \Delta_1 + \Delta_2 + \lambda + \theta, \quad G = \Delta_1 - \Delta_2 + \lambda + \theta,$$

$$\lambda = \frac{\hbar^2}{2m_0}[A_1 k_z^2 + A_2(k_x^2 + k_y^2)] + D_1\epsilon_{zz} + D_2(\epsilon_{xx} + \epsilon_{yy}),$$

$$\theta = \frac{\hbar^2}{2m_0}[A_3 k_z^2 + A_4(k_x^2 + k_y^2)] + D_3\epsilon_{zz} + D_4(\epsilon_{xx} + \epsilon_{yy}),$$

$$K = \frac{\hbar^2}{2m_0}A_5(k_x + ik_y)^2 + D_5(\epsilon_{xx} - \epsilon_{yy} + 2i\epsilon_{xy}),$$

$$H = \frac{\hbar^2}{2m_0}i[A_6 k_z(k_x + ik_y) + A_7(k_x + ik_y)] + iD_6(\epsilon_{xz} + i\epsilon_{yz}),$$

$$I = \frac{\hbar^2}{2m_0}i[A_6 k_z(k_x + ik_y) - A_7(k_x + ik_y)] + iD_6(\epsilon_{xz} + i\epsilon_{yz}),$$

$$\Delta = \sqrt{2}\Delta_3. \tag{2}$$

$D_1$-$D_6$ are the deformation potentials and $A_1$-$A_7$ are the fitting parameters to valence band structures. $k_i$ and $\epsilon_{ij}$ $(i,j=x,y,z)$ are the wave vector and the strain tensor. $\Delta_1$ is the crystal-field energy. $\Delta_2$ and $\Delta_3$ are the spin-orbit energy parameters. The parameters can be found in Refs. 3 and 26, and all main parameters we used are listed in Table I. The growth direction of $a$-plane quantum well is $x$-direction. Therefore, the $k_x$ will be transformed into the differential forms $-i\partial/\partial x$. Due to the out-of-plane stress component $\sigma_{xx}=0$, the out-of-plane strain $\epsilon_{xx}$ can be expressed as

$$\epsilon_{xx} = -\frac{C_{12}}{C_{11}}\epsilon_{yy} - \frac{C_{13}}{C_{11}}\epsilon_{zz}, \tag{3}$$

where $C_{ij}$ are the elastic stiffness constants.

The bases of the Hamiltonian are $1/\sqrt{2}|X+iY,\uparrow\rangle$, $1/\sqrt{2}|X+iY,\downarrow\rangle$, $|Z,\uparrow\rangle$, $|Z,\downarrow\rangle$, $1/\sqrt{2}|X-iY,\uparrow\rangle$, and $1/\sqrt{2}|X-iY,\downarrow\rangle$, where the polarization of the emission light is strongly affected by these bases.

We apply the self-consistent Poisson and $6\times6$ $k\cdot p$ Schrödinger solver to iteratively solve the band structure, energy levels, and wave functions of electron and hole until they are converged. Then we use Eq. (4) to acquire the polarization-dependent optical matrix element,

$$x\text{-polarized}: |\langle S|p_x|X\rangle|^2(|\langle\psi_l^e|\psi_{m1}^h\rangle\uparrow + \langle\psi_l^e|\psi_{m5}^h\rangle\uparrow|^2 + |\langle\psi_l^e|\psi_{m2}^h\rangle\downarrow + \langle\psi_l^e|\psi_{m6}^h\rangle\downarrow|^2)/4$$

TABLE I. Physical parameters of GaN and InN.

| Parameters | GaN | InN |
|---|---|---|
| Lattice constant ($T$=300 K) | | |
| $a$ (Å) | 3.189[a] | 3.545[a] |
| $c$ (Å) | 5.185[a] | 5.703[a] |
| Valence band effective mass parameters | | |
| $A_1$ | −6.56[b] | −8.21[a] |
| $A_2$ | −0.91[b] | −0.68[a] |
| $A_3$ | 5.65[b] | 7.57[a] |
| $A_4$ | −2.83[b] | −5.23[a] |
| $A_5$ | −3.13[b] | −5.11[a] |
| $A_6$ | −4.86[b] | −5.96[a] |
| Deformation potentials (eV) | | |
| $D_1$ | −1.7[c] | −1.76[c] |
| $D_2$ | 6.3[c] | 3.43[c] |
| $D_5$ | −4.0[c] | −2.33[c] |
| $D_6$ | −5.5[a] | −5.5[a] |
| $D_3=D_2-D_1$, $D_4=-D_3/2$ [d] | | |
| Energy parameters (meV) | | |
| $\Delta_1$ | 22.0[c] | 41.0[c] |
| $\Delta_2=\Delta_3$ | 5.0[c] | 0.333[c] |
| Elastic constant ($10^{11}$ dyn/cm$^2$) | | |
| $C_{11}$ | 39.0[e] | 27.1[f] |
| $C_{12}$ | 14.5[e] | 12.4[f] |
| $C_{13}$ | 10.6[e] | 9.4[f] |
| $C_{33}$ | 39.8[e] | 20.0[f] |
| $C_{44}$ | 10.5[e] | 4.6[f] |
| $C_{66}$ | 12.3[e] | 7.4[f] |

[a]Reference 26.
[b]Reference 29.
[c]Reference 3.
[d]Reference 30.
[e]Reference 31.
[f]Reference 32.

$$y\text{-polarized}: |\langle S|p_y|Y\rangle|^2(|\langle\psi_l^e|\psi_{m1}^h\rangle\uparrow - \langle\psi_l^e|\psi_{m5}^h\rangle\uparrow|^2 + |\langle\psi_l^e|\psi_{m2}^h\rangle\downarrow - \langle\psi_l^e|\psi_{m6}^h\rangle\downarrow|^2)/4$$

$$z\text{-polarized}: |\langle S|p_z|Z\rangle|^2(|\langle\psi_l^e|\psi_{m3}^h\rangle\uparrow + \langle\psi_l^e|\psi_{m4}^h\rangle\downarrow|^2)/2. \tag{4}$$

After obtaining $|\hat{a}\cdot\vec{p}_{i,j}|^2$ from Eq. (4), we can determine the polarization-dependent spontaneous emission rate. The light emission rate is expressed as

$$R_{sp} = \int d(\hbar\omega)\frac{e^2 n_r \hbar\omega}{m_0^2\varepsilon_0 c^3\hbar^2}\sum_{i,j}\int\frac{2}{(2\pi)^2}d^2\vec{k}|\hat{a}\cdot\vec{p}_{i,j}|^2 \times \frac{1}{\sigma\sqrt{2\pi}}\exp\left[\frac{-(E_{i,j}-\hbar\omega)^2}{2\sigma^2}\right]f^e[E_i^e(\vec{k})]f^h[E_j^h(\vec{k})]$$

$$(\text{cm}^{-2}\,\text{eV}^{-1}\,\text{s}^{-1}), \tag{5}$$

where $f^e$ and $f^h$ are Fermi–Dirac function, $n_r$ is the refractive index, and $E_{i,j}$ is the effective bandgap from state $i$ and $j$. $\sigma$ is the inhomogeneous broadening factor.

In order to analyze the polarization, we need to define the polarization ratio. The definition of polarization ratio is

$$\rho = \frac{I_y - I_z}{I_y + I_z}, \tag{6}$$

where $I_y$ and $I_z$ are the emission intensity with polarization parallel to the $y$-axis and $z$-axis, respectively.[6,27]

## III. RESULTS

The light emission in the semiconductor material is generated by the electron transition from the conduction band to the valence band. As we know, the conduction band is mainly formed by the $|s\rangle$ core state, which is a spherically symmetric orbital. The valence bands are mainly formed by the $|p_x\rangle$, $|p_y\rangle$, and $|p_z\rangle$ atomic orbitals. When the transition occurs between the $|s\rangle$ state and $|p_x\rangle$, $|p_y\rangle$, and $|p_z\rangle$ valence band states, the light emission from these kinds of transitions will be $x$-polarized, $y$-polarized, and $z$-polarized light, respectively.

In the $c$-plane InGaN/GaN quantum well system, the topmost CH1 and CH2 states are formed by $|X+iY\rangle$ and $|X-iY\rangle$, respectively. Due to the in-plane symmetric atom distribution in wurtzite structure, the in-plane strain of $c$-plane InGaN/GaN quantum well is isotropic. As a result, the $|X\rangle$ state and $|Y\rangle$ state of CH1 and CH2 bands are still equally mixed to each other under strained condition. Hence, if we consider the light emission toward the surface (along $c$-axis), the emitted light would be nonpolarized since the $x$-polarized light is equal to the $y$-polarized light.

However, if we rotate the growth direction to the nonpolar $a$-plane orientation, the in-plane strain will become anisotropic. Due to the anisotropic strain, the original $|X+iY\rangle$ and $|X-iY\rangle$ states are separated into $|X\rangle$-like and $|Y\rangle$-like states. It is important to note that since the valence band structure is strongly modified, the $|Y\rangle$-like state becomes the topmost state. Therefore, a strong polarized light emission will be measured at the growth direction (along $x$-axis). Also, in order to achieve larger polarization ratio, we need to control the energy separation of $|Y\rangle$-like and $|Z\rangle$-like states as large as possible.

As mentioned earlier, the quantum well width strongly affects the energy separation of the different states. The influence of the energy separation with different quantum well widths is depending on the effective mass along the growth direction. Figure 1 shows the calculated valence band structure of $a$-plane bulk $In_{0.2}Ga_{0.8}N$ material with $6\times6$ $k\cdot p$ method. The effects of biaxial strain for $In_{0.2}Ga_{0.8}N$ grown on GaN is considered here. Figure 1(a) shows the $E$-$k$ curve along the $k_x$ and $k_y$ directions. We can find that due to the asymmetric strain, the $|X\rangle$-like state is lowering down, which has much smaller effective mass along the $k_x$ direction. The $|Y\rangle$-like and $|Z\rangle$-like states are stayed at the top. The effective mass of the $|Z\rangle$-like state ($\sim1.176m_0$) is slightly smaller than that of the $|Y\rangle$-like state ($\sim1.731m_0$) along the $k_x$ direction. Therefore, we can expect that after making the quantum well, the $|Y\rangle$-like and $|Z\rangle$-like states will remain on top since they have larger effective mass along the $k_x$ direction compared to $|X\rangle$-like. The separation of the $|Y\rangle$-like and $|Z\rangle$-like states will become larger with strong quantum confinement effect and the different effective masses. Figure 1(b) shows the $E$ versus $k$ relation along the $k_y$ and $k_z$ directions. We can find that the CH1 band is mainly dominated by $|Y\rangle$-like state. It can be seen that the band-edge effective mass of the CH1 state along the $k_z$ direction ($\sim1.142m_0$) is larger than that along the $k_y$ direction ($\sim0.136m_0$). The CH2 band is dominated by $|Z\rangle$-like state. With the smaller $k$ vector, the energy is lower than CH1 band. Therefore, the polarization will be mainly $y$-polarized light. However, along the $k_y$ direction, the energy of $|Z\rangle$-like state will be higher than $|Y\rangle$-like state when the $k_y$ value is larger than 0.04 $Å^{-1}$, where the polarization ratio will become smaller.

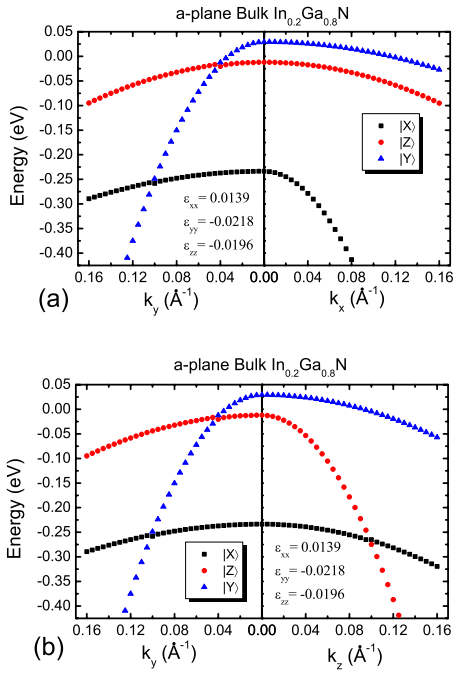


FIG. 1. (Color online) The valence band structure under strained condition of $a$-plane bulk $In_{0.2}Ga_{0.8}N$ material along (a) the $k_x$ direction and the $k_y$ direction and (b) along the $k_y$ direction and the $k_z$ direction.

When we start to consider the quantum confinement effect from quantum well, the energy separation of each band will not be affected only by the epitaxial strain from lattice mismatch but also by the quantum confinement effect. As mentioned earlier, a self-consistent Poisson and Schrödinger $k\cdot p$ solver is applied in the study. Figures 2(a) and 2(b) show the change of polarization ratio and energy separation between the first $|Y\rangle$-like and $|Z\rangle$-like subbands versus quantum well width with different indium compositions, respectively. As shown in Fig. 2(a), the polarization ratio of light increases with smaller quantum well width. Also, with larger indium composition, the polarization ratio increases as well. If we look at the energy separation of each subband with different quantum well widths, we find that the change of polarization ratio and the energy separation have similar trend, which would be the result of the quantum confinement effect. The improvement with smaller quantum well width is not significant because of the small effective mass difference along the confined $k_x$ direction as we mentioned earlier. Therefore, if we want to enhance the effect of quantum confinement, we need to find a growth direction, which can provide a larger effective mass differences, such as semipolar devices.

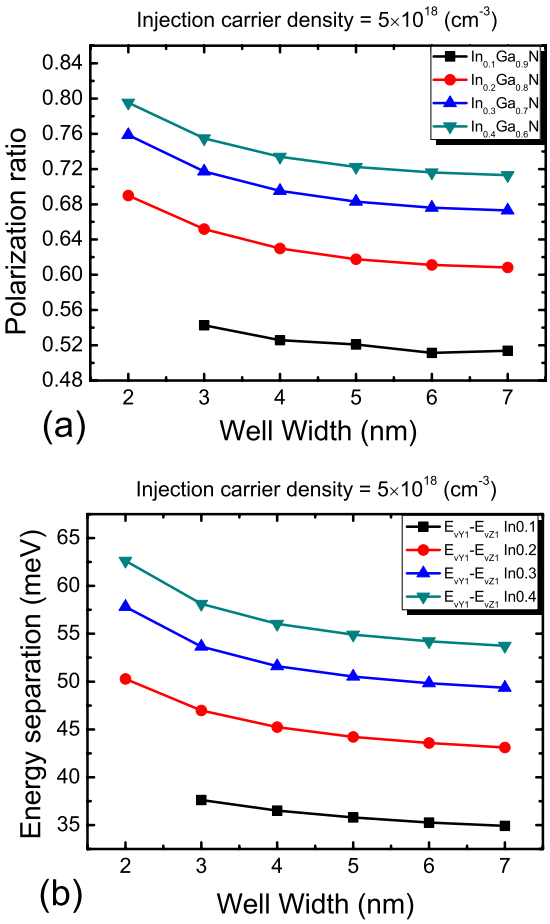


FIG. 2. (Color online) (a) The polarization ratio as a function of well width with different indium compositions. (b) The energy separation of the first $|Y\rangle$-like subband to the first $|Z\rangle$-like subband state as a function of well width with different indium compositions.

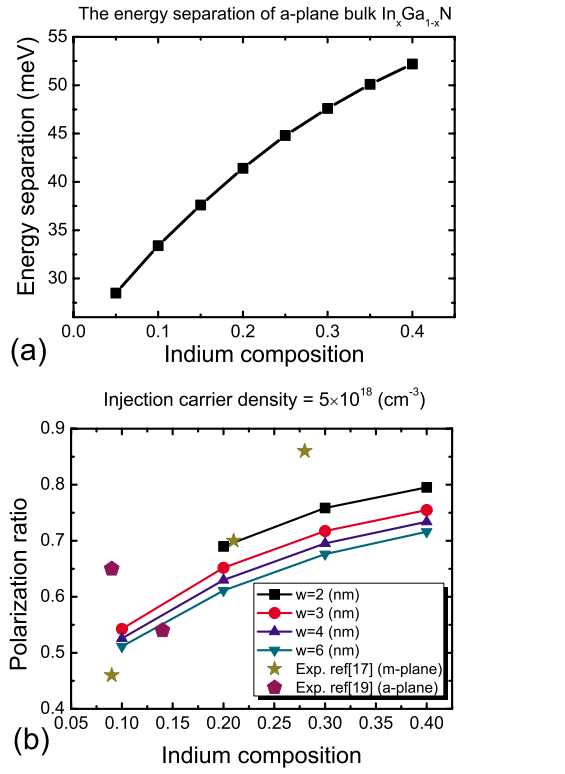


FIG. 3. (Color online) (a) The energy separation of $|Y\rangle$-like to $|Z\rangle$-like state as a function of indium composition of $a$-plane bulk $In_xGa_{1-x}N$ material with strained condition. (b) The polarization ratio of InGaN/GaN $a$-plane quantum well as a function of indium composition with different well widths. Note that there is no confined subband found for $W=2$ nm with 10% indium composition. The experimental works of $m$-plane (Ref. 17) and $a$-plane (Ref. 19) are listed for comparison.

We can find that the polarization ratio increases as the indium composition increases, as shown in Fig. 2(a). This may be due to the combination of quantum confinement effect and strain induced energy separation. As we know, the increase in the indium composition leads to the increase in strain effect. Figure 3(a) shows the calculated energy separation of bulk InGaN under biaxial strain in the $a$-plane. The quantum confinement effect is not included. Due to the asymmetric strain in $x$- (growth direction) and $y$-directions, the original $|X+iY\rangle$ state is separated into $|X\rangle$-like and $|Y\rangle$-like states. The $|Y\rangle$-like state is raised, while the $|X\rangle$-like is lowered due to the anisotropic compressive strain ($\epsilon_{xx} \neq \epsilon_{yy}$).[25] We can find that as the indium composition increases, the energy separation of the $|Y\rangle$-like state to $|Z\rangle$-like state continues to increase,[28] as shown in Fig. 3(a). Hence, the $y$-polarized light emitted from the transition between $|S\rangle$-state and $|Y\rangle$-state is dominant. As a result, the polarization ratio increases as indium composition increases, as shown in Fig. 3(b).

We also compared our simulation results with published experimental works. Most experimental works on polarization ratio studies are mainly for $m$-plane[14–17] and few works on $a$-plane.[19] From Eqs. (1) and (2), we can find that the difference between $m$-plane and $a$-plane InGaN quantum well is that $|X\rangle$-like state will lift up for $m$-plane, and $|Y\rangle$-like state will lift up for $a$-plane. However, the polarization ratio changes will be the same. As shown in Fig. 3(b), the polarization ratio of the experimental results for $m$-plane monotonically increases with the indium composition, as predicted by our calculation. For the $a$-plane results, the polarization ratio for samples with 9% and 14% indium composition is close to our prediction. However, the polarization ratio does not increase with the indium composition due to the growth quality of samples, where In-clustering localized states are formed. As mentioned in Ref. 19, the growth quality for $a$-plane InGaN quantum well still needs improvements. Finally, it is worth noting that in experiments, the actual carrier density in the quantum well may not be the same as that used in calculations, and therefore the measured and calculated polarization ratios will not be exactly the same.

Figure 4 shows the change in polarization ratio and Fermi level versus injection carrier density. Even though it does not modify the valence band structure too much by increasing injection carrier density, it affects the population of carriers in each subband. When more carriers are injected into the quantum well, the higher energy states are filled with carriers. As a result, there are more carriers being filled in $|Z\rangle$-like state under the high injection condition compared to the low injection condition. The $z$-polarized light component increases as the carrier injection density increases. Therefore, the polarization ratio decreases under high carrier injection condition. Similar effects are also observed by experimental results.[17]

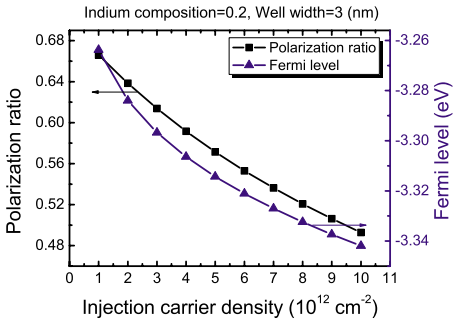


FIG. 4. (Color online) The shift of the polarization ratio and Fermi level vs the injection carrier density.

Figure 5 shows the valence band structure of $In_{0.2}Ga_{0.8}N/GaN$ $a$-plane quantum well along the $k_y$ and the $k_z$ directions. As mentioned before, the energy separation of the two topmost states is strongly related to the strain and quantum confinement effect, which will modify the valence band structure. It can be seen that the energy separation of the $a$-plane quantum well valence band structure is larger than that for the conventional $c$-plane quantum well. Also, we can find the asymmetric behavior along the $k_y$ and $k_z$ directions. For the first and the second subbands ($|Y\rangle$-like state), the effective masses are large along the $k_z$ direction and much smaller along the $k_y$ direction. However, for the third subband ($|Z\rangle$-like state), the effective mass is large along the $k_y$ direction and much smaller along the $k_z$ direction. Therefore, along the $k_y$ direction, there are two interception points at $k_y$ close to 0.008 Å$^{-1}$ and 0.044 Å$^{-1}$, respectively. Hence, when carriers are filling the ground state with larger $k_y$ value, the ground state will become $|Z\rangle$-like state dominated. Along the $k_z$ direction, since the $|Z\rangle$-like state has smaller effective mass, the polarization ratio will be greatly enhanced when the carrier filling the larger $k_z$ states.

Figure 6(a) shows the optical matrix element of $|y\rangle$ and $|z\rangle$ components in the first subband versus $k_z$. As mentioned earlier, the optical matrix element of $y$-polarized light increases as the $k_z$ increases. On the other hand, the optical matrix element of $z$-polarized light decreases as the $k_z$ increases. However, due to the mixing between the topmost states is weak, the $y$-polarized light is dominated in the whole $k_z$ direction. Therefore, the ratio of $y$-polarization to $z$-polarization increases as the $k_z$ increases, as shown in Fig. 6(b).

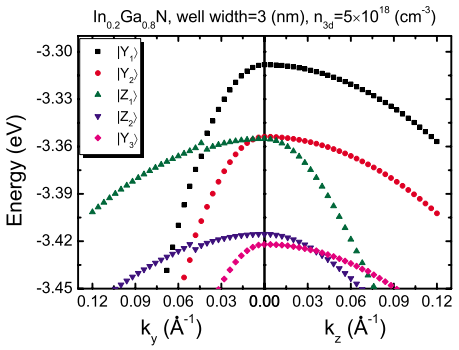


FIG. 5. (Color online) The valence band dispersion relation of the $In_{0.2}Ga_{0.8}N/GaN$ $a$-plane quantum well.

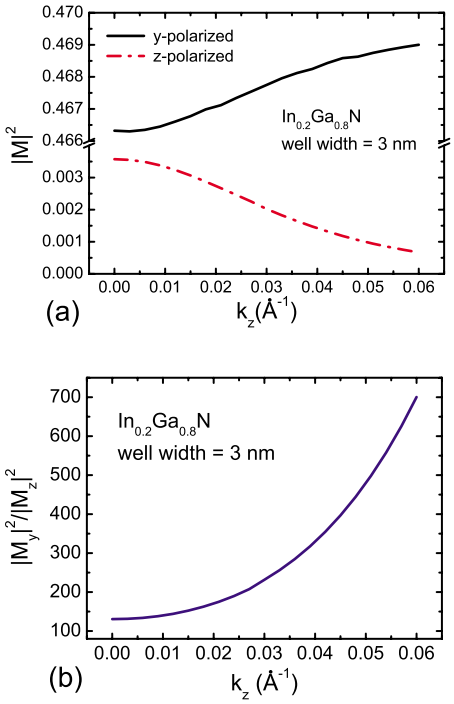


FIG. 6. (Color online) (a) The optical matrix element of $|y\rangle$ and $|z\rangle$ components in the first subband vs $k_z$. (b) The ratio $|M_y|^2/|M_z|^2$ in the first subband vs $k_z$.

However, since the lattice distribution in $y$-$z$ plane of the wurtzite structure is asymmetric, the dispersion relation along the $k_y$ direction is totally different. As shown in Fig. 5, there exists a strong mixing state coupling when the $k_y$ is close to 0.044 Å$^{-1}$, and it is noted that the $|Y\rangle$ and $|Z\rangle$ states are equally mixed to each other when the $k_y$ value is equal to 0.0432 Å$^{-1}$. When the $k_y$ value is larger than 0.044 Å$^{-1}$, the ground state is then dominated by $|Z\rangle$-like state. Hence, as shown in Figs. 7(a) and 7(b), we obtain the inverse results of optical matrix element for $y$-polarization and $z$-polarization along the $k_y$ direction. For carriers injected into the $a$-plane quantum well to fill the states along the $k_y$ and the $k_z$ directions, the behaviors of polarization ratio changes are totally different, which make the design of polarized light source much difficult.

## IV. CONCLUSION

In conclusion, the influences of the indium composition, well width, and injection carrier density to the $a$-plane quantum well are studied in this work. Our results show that the smaller quantum well width and the higher indium composition increase the polarization ratio. However, if the device is operated under high carrier injection conditions, we need to concern about the variation of optical matrix element in different $k$ directions near Γ point. As a result, the polarization ratio decreases when we increase the carrier injection. Some published experimental works are compared to our calculation and have shown a good agreement with our work. We have studied the different conditions for designing the $a$-plane InGaN quantum well LED for applications, such as LCD backlight modules and lasers, which would be useful information for device designs. In the future work, our stud-

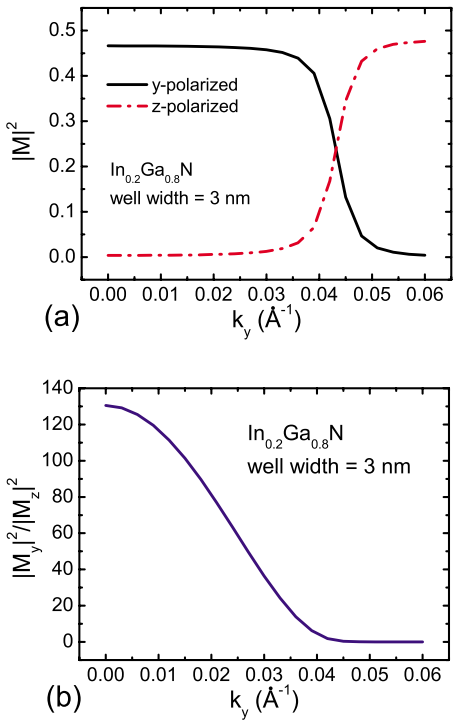


FIG. 7. (Color online) (a) The optical matrix element of $|y\rangle$ and $|z\rangle$ components in the first subband vs $k_y$. (b) The ratio $|M_y|^2/|M_z|^2$ in the first subband vs $k_y$.

ies show that to enhance the quantum confinement effect with different quantum well widths, the effective mass difference along confined direction should be large. Therefore, we will look for semipolar device in arbitrary angle to find the best enhancement of polarization ratio.

## ACKNOWLEDGMENTS

The authors would like to thank National Science Council in Taiwan for the financial support, under Grant Nos. NSC-97-2221-E002-050 and 97-2623-7-002-018-ET, and the financial support from Ministry of Education in the project "Aim for Top University".

[1]K. C. Kim, M. C. Schmidt, H. Sato, F. Wu, N. Fellows, Z. Jia, M. Saito, S. Nakamura, S. P. DenBaars, J. S. Speck, and K. Fujito, Appl. Phys. Lett. **91**, 181120 (2007).
[2]H. Masui, H. Yamada, K. Iso, J. S. Speck, S. Nakamura, and S. P. DenBaars, J. Soc. Inf. Disp. **16**, 571 (2008).
[3]S. H. Park, D. Ahn, and S. L. Chuang, IEEE J. Quantum Electron. **43**, 1175 (2007).
[4]S. H. Park, D. Ahn, and J. E. Oh, Appl. Phys. Lett. **92**, 011130 (2008).
[5]A. A. Yamaguchi, Jpn. J. Appl. Phys., Part 2 **46**, L789 (2007).
[6]K. Kojima, H. Kamon, M. Funato, and Y. Kawakami, Phys. Status Solidi C **5**, 3038 (2008).
[7]S. Khatsevich and D. H. Rich, J. Phys.: Condens. Matter **20**, 215223 (2008).
[8]S.-H. Park, J. Appl. Phys. **91**, 9904 (2002).
[9]H. Masui, A. Chakraborty, B. A. Haskell, U. K. Mishra, J. S. Speck, S. Nakamura, and S. P. DenBaars, Jpn. J. Appl. Phys., Part 2 **44**, L1329 (2005).
[10]K. Okamoto, H. Ohta, D. Nakagawa, M. Sonobe, J. Ichihara, and H. Takasu, Jpn. J. Appl. Phys., Part 2 **45**, L1197 (2006).
[11]S. Nakagawa, H. Tsujimura, K. Okamoto, M. Kubota, and H. Ohta, Appl. Phys. Lett. **91**, 171110 (2007).
[12]H. Masui, M. C. Schmidt, K. C. Kim, A. Chakraborty, S. Nakamura, and S. P. Denbaars, Jpn. J. Appl. Phys., Part 1 **46**, 7309 (2007).
[13]Y. J. Sun, O. Brandt, M. Ramsteiner, H. T. Grahn, and K. H. Ploog, Appl. Phys. Lett. **82**, 3850 (2003).
[14]N. F. Gardner, J. C. Kim, J. J. Wierer, Y. C. Shen, and M. R. Krames, Appl. Phys. Lett. **86**, 111101 (2005).
[15]T. Koyama, T. Onuma, H. Masui, A. Chakraborty, B. A. Haskell, S. Keller, U. K. Mishra, J. S. Speck, S. Nakamura, S. P. DenBaars, T. Sota, and S. F. Chichibu, Appl. Phys. Lett. **89**, 091906 (2006).
[16]H. Tsujimura, S. Nakagawa, K. Okamoto, and H. Ohta, J. J. Appl. Phys. Part 2 **46**, L1010 (2007).
[17]H. Masui, H. Yamada, K. Iso, S. Nakamura, and S. P. DenBaars, J. Phys. D: Appl. Phys. **41**, 225104 (2008).
[18]T. S. Ko, T. C. Lu, T. C. Wang, J. R. Chen, R. C. Gao, M. H. Lo, H. C. Kuo, S. C. Wang, and J. L. Shen, J. Appl. Phys. **104**, 093106 (2008).
[19]C. H. Chiu, S. Y. Kuo, M. H. Lo, C. C. Ke, T. C. Wang, Y. T. Lee, H. C. Kuo, T. C. Lu, and S. C. Wang, J. Appl. Phys. **105**, 063105 (2009).
[20]T. Ohtoshi, A. Niwa, and T. Kuroda, Jpn. J. Appl. Phys. Part 2 **35**, L1566 (1996).
[21]J. Bhattacharyya, S. Ghosh, and H. T. Grahn, Appl. Phys. Lett. **93**, 051913 (2008).
[22]M. V. Kisin, R. G. W. Brown, and H. S. El-Ghoroury, Appl. Phys. Lett. **94**, 021108 (2009).
[23]Y.-R. Wu, Y.-Y. Lin, H.-H. Huang, and J. Singh, J. Appl. Phys. **105**, 013117 (2009).
[24]Y.-R. Wu, C. Chiu, C.-Y. Chang, P. Yu, and H.-C. Kuo, IEEE J. Sel. Top. Quantum Electron. **15**, 1 (2009).
[25]S. Ghosh, P. Waltereit, O. Brandt, H. T. Grahn, and K. H. Ploog, Phys. Rev. B **65**, 075202 (2002).
[26]I. Vurgaftman and J. R. Meyer, J. Appl. Phys. **94**, 3675 (2003).
[27]H. Yamada, K. Iso, M. Saito, H. Masui, K. Fujito, S. P. DenBaars, and S. Nakamura, Appl. Phys. Express **1**, 041101 (2008).
[28]M. Kubota, K. Okamoto, T. Tanaka, and H. Ohta, Appl. Phys. Lett. **92**, 011920 (2008).
[29]S. L. Chuang and C. S. Chang, Phys. Rev. B **54**, 2491 (1996).
[30]M. Kumagai, S. Chuang, and H. Ando, Phys. Rev. B **57**, 15303 (1998).
[31]S. H. Park and S. L. Chuang, J. Appl. Phys. **87**, 353 (2000).
[32]K. Kim, W. R. L. Lambrecht, and B. Segall, Phys. Rev. B **53**, 16310 (1996).